SPONSORED BY THE
Federal Ministry of Education and Research

Finanziert von der Europäischen Union
NextGenerationEU

DEDICATED DESIGN OF THE FREE JETS FOR ROTARY SLIDE VALVES

Lennard Günther*, Sven Osterland, Danny Staroszyk, Jürgen Weber

Institute of Mechatronic Engineering, Technische Universität Dresden, Helmholtzstrasse 7a, 01069 Dresden
* Corresponding author: Tel.: +49 351 463-39200; E-mail address: Lennard.guenther@tu-dresden.de

ABSTRACT

The paper presents a general analytical method for the determination of the flow angel in hydraulic components like valves and pumps. In this paper it will be illustrated by a rotary slide valve.
The design of the flow geometry e.g. in valves depends on many influencing parameters. A suitable choice of parameters ensures that target variables such as flow characteristics, flow force, but also other effects such as cavitation and noise generation can be improved. An important parameter is the flow angle of the free jet, which forms in each valve directly downstream of the narrow section of the control edge. The resulting free jet influences the flow force as well as cavitation damage. By a suitable choice of the angle of this free jet, the flow force can be reduced by changing the direction of the outgoing impulse. With regard to cavitation, the impact of the free jet can be shifted and thus the cavitation erosion can be shifted or weakened. However, the flow angle is not always known and the influence of the parameter cannot be fully exploited. In the past, numerous elaborate experimental investigations or simulations have been carried out to improve influencing parameters on corresponding target sizes, as just mentioned. In many cases, the decisive factor is the flow angle of the emerging free jet.
This paper deals with the investigation of the flow angle of free jets as well as the technical application on the basis of rotary slide valves. In the first section, geometric factors influencing the flow angle are discussed, as well as the transferability of the results under varying operating conditions (laminar and turbulent). Using a generic minimal model, the behavior of the flow angle with respect to geometric influence factors and operating conditions is investigated by means of CFD. The results are adapted to the real application, a rotary slide valve. Direct adjustment of the flow angle results in a significant improvement in the resistance torque caused by the flow force. It becomes clear how efficient the adjustment of the flow angle can be if the basis of the formation of the free jet is known. Due to the derivation of the relationship with the help of an abstracted minimal model, the knowledge gained can be used in many ways and can also be transferred to other applications in the field of fluid technology. Optimization processes are more efficiently without using elaborated models e.g. driven by CFD.

Keywords: flow angle, free jet, rotary slide valve, design process

1. INTRODUCTION

The flow angle of the free jet plays a decisive role in the functionality and performance of fluid power components. Internal flows, which are common in hydraulics, have a large number of abrupt cross-sectional constrictions. At those narrow points, e.g. at control edges of valves, a free

jet is formed as the flow passes through. This free jet influences the resulting flow force acting on the valve spool [1]. In addition, the free jet has a great influence on the formation and transport of cavitation bubbles. In the shear layers of the free jet, vortices are formed in which the bubbles are created and grow [2]. The bubbles are transported with the flow and collapse if the local pressure increases again, e.g. at stagnation points. In areas close to the wall, this leads to a microjet. That causes erosion damage to the component, shown in [1] and [3]. However, free jets also occur in pumps such as the valve plate of an axial piston pump, during the transition from low pressure to high pressure, which can cause cavitation damage [4]. Depending on the geometry, the free jet aligns itself via the flow angle. The literature on specific angle positions is long. In [1], the angle for individual control positions of a spool valve is defined. Similarly, the flow angles are described for example by [5], [6], [7], [8], where all data on the angle correlate well with an acceptable scatter. In [9] and [10] the clearance at the valve spool and the sleeve are considered, which is important for very small opening ratios.

A common question during the valve and pump development process is: In what way is the flow angle affected by the control edge geometry? This paper deals with the investigation of the flow angle by using a generic minimal model. The aim is a general method about how the flow angle results from geometric parameters and in which operating range it is valid. The transfer of the results to a real application reflects the applicability of the obtained correlation. The implementation is carried out using a rotary slide valve, which is illustrated in **Figure 1**. As a special design compared to conventional rotary slide valves, this one is integrated into a cartridge installation space. The valve can be operated in both flow directions. The illustration shows for example of the flow direction the inlet horizontally and the outlet vertically on the bottom. The valve has three control edges in the horizontal plane, which are offset by 120 °. A complete opening and closing process takes place at a twisting angle φ of 0 ° (fully open) to 60 ° (closed). The aim is to optimize the flow forces by actively influencing the flow angle of the free jet.

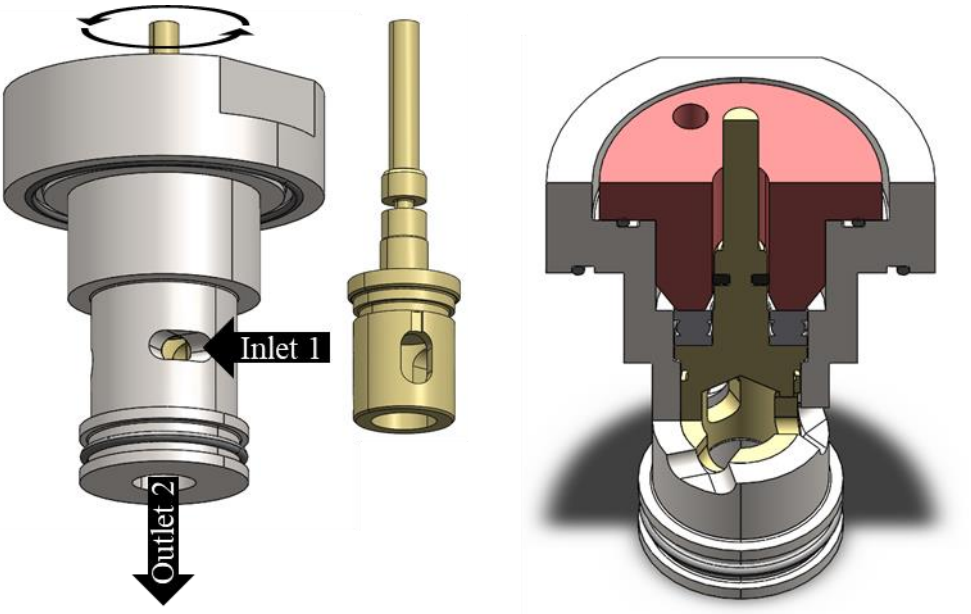

Figure 1: Rotary slide valve, exemplary flow direction 1 → 2 through the assembly (left), valve spool (middle), sectional view through the inlet plane and the vertical center plane (right)

2. METHODOLOGY

The flow force calculation can be done in different ways. A simple and in most cases effective method is the determination of the resulting force using the conservation of momentum. Another advantage is that the dependencies can be easily identified through such an analytical relationship. For a defined control volume Ω, time-dependent (I), incoming and outgoing (II) momentum, as well as pressure forces (III) and shear forces (IV) or volume-dependent forces, such as acceleration forces (V), and body forces (VI) can be taken into account via the boundary S. As shown in Eq. (1), the complete relation of the conservation of momentum is described in integral form.

$$\underbrace{\int_{\Omega} \frac{\partial \rho \vec{u}}{\partial t} dV}_{I} + \underbrace{\int_{S} \rho \vec{u} \, (\vec{u} \cdot \vec{n}) dS}_{II} = \underbrace{- \int_{S} p \vec{n} dS}_{III} + \underbrace{\int_{S} \bar{\bar{\tau}} \cdot \vec{n} dS}_{IV} + \underbrace{\int_{\Omega} \rho \vec{f} dV}_{V} + \underbrace{\vec{F}_B}_{VI} \tag{1}$$

For the hydraulic application concerning the rotary slide valve, the following simplification can be assumed, which reduces the expression, **Figure 2**.

Steady state: $\frac{\partial}{\partial t} = 0$

Pressure compensated: $\int_S p \vec{n} dS = 0$

Flows close to the wall are very small compared to the resulting body forces ($\vec{F}_{\bar{\tau}} \ll \vec{F}_B$) [11]: $\int_S \bar{\bar{\tau}} \cdot \vec{n} dS = 0$

Movement of the volume is neglected: $\int_{\Omega} \rho \vec{f} dV = 0$

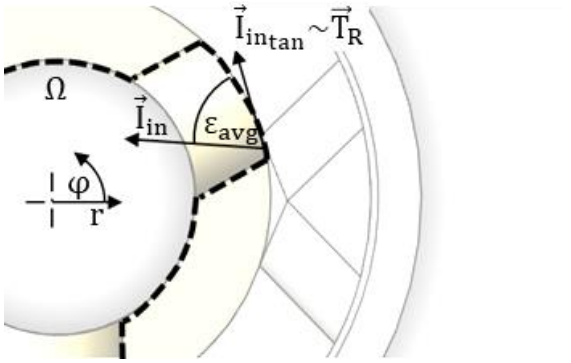

Figure 2: Application of the law of conservation of momentum on the basis of the rotary slide valve, valve spool (yellow), housing (light gray), control volume Ω (black, dashed).

This results in an equation that describes only the dynamic part of the flow. The momentum entering and leaving the control volume determine it.

$$\int_{\check{S}} \rho \vec{u} \, (\vec{u} \cdot \vec{n}) dS = \vec{F}_B \tag{2}$$

Eq. (2) can be explained in cylindrical coordinates, Eq. (3). Thus, it becomes easier to apply to the control volume of the rotary slide valve. The momentum of the outlet is perpendicular to the flow over the control edge. Thus there is no influence in the equations.

$$F_{flow} = \rho \left| \vec{u}_{in}^2 \right| \cdot A_{in} \cdot \cos(\varepsilon_{avg}) \tag{3}$$

$$T_R = \int F_{flow} \, dr = \rho \left| \vec{u}_{in}^2 \right| \cdot A_{in} \cdot r \cos(\varepsilon_{avg}) \tag{4}$$

Eq. (3) defines the flow force and (4) the resistance torque acting tangential on the valve spool per control edge. As already mentioned, it is easy to see that the resistance torque T_R as well as the flow force F_{flow} depend on the geometric parameters of the flow area A_{in} and the averaged flow angle ε_{avg}. Since the area cannot be used as an influencing parameter in this case because it must necessarily be opened to release the flow cross section. Only the flow angle remains to actively influence the resistance torque of the flow at the control edge / narrow section.

But how does the flow angle behave and how can it be influenced? In the following, the methodology for investigating and derivation will be explained.

Due to the lack of knowledge about the exact behavior of the flow angle, the correlation is examined in a generic minimal model by using CFD. The geometry is selected in such a way that no disturbance effects can influence the flow. The focus is purely on the variation of the flow angle. It is shown in [1], that the flow angle has a significant dependency of the inlet geometry.

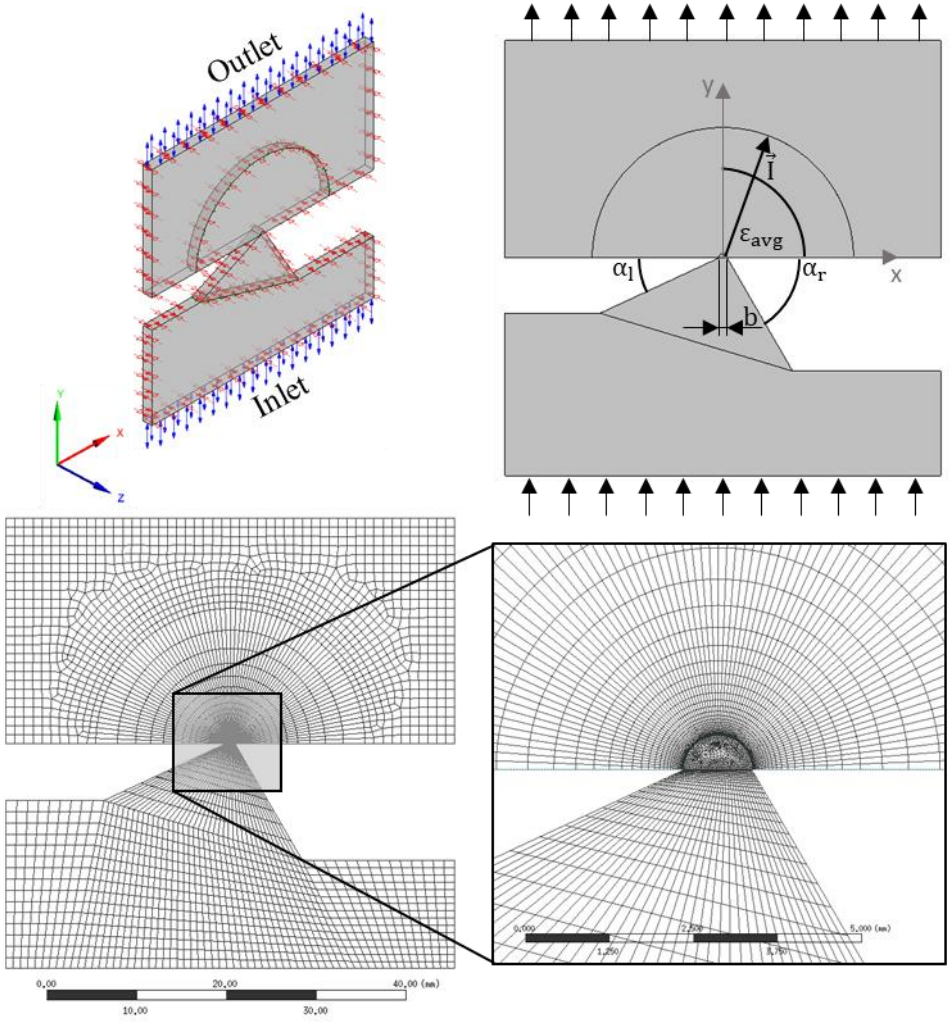

Figure 3: Overview of geometry of the model (top) and representation of meshing (overview - bottom left, bottleneck - bottom right).

Figure 3 illustrates the flow simulation model, which is used to study the flow angle. The geometry is divided into inflow area (lower region), narrow section (center) and outflow area (upper region). The inlet region is variable using the angles α_l and α_r of the left and right walls. Thus, the flow angle of the free jet in the narrow section can be changed. The narrow section has

a fixed width b of 1 mm and is arranged horizontally. The outlet region spans a free space starting from the narrow section in which the jet can spread freely. Due to many symmetrical relationships in technical geometries, a two-dimensional model is used for this investigation. The setup of the simulation model is summarized in **Table 1**. With the aid of this model, a new analytical method will be established to determine the flow angle at a narrow section very well (ch. 3.3, Eq. (13)). The correlation shows a simplified expression between the inlet geometry and the flow angle of the free jet. The comparison of a real application is made in ch. 4 by using the rotary slide valve.

Table 1: minimal model - setup

property	setting	property	setting
geometrical variation		analysis type	
α_l	$\{0 \dots 180\}°$	temporal consideration	steady state
α_r	$\{0 \dots 180\}°$	turbulence	Shear Stress Transport model (RANS)
b	1 mm	convergence	
boundary conditions		convergence criterion	10^{-4}
inlet	opening with $p_{in} = \{10^{-4} \dots 10^{2}\}$ bar	max. number of time steps	200
outlet	opening with $p_{out} = 0$ bar	fluid properties	
wall	no slip wall (geometry related to x-y-plane)	density	863 kg / m³, incompressible
symmetry	in z-direction	kin. viscosity	46 mm² / s
		temperature	40 °C, isotherm

3. FLOW ANGLE OF FREE JETS ON THE MINIMAL MODEL

This chapter deals with the study of the properties and derivation of the flow angle. For a better understanding, the following structure is used.

- general definition of the local and averaged flow angle
- laminar and turbulent influence
- analytical method for the averaged flow angle

3.1. Definition of the flow angle ε

The local flow angle ε_{loc} at a given point in the fluid domain is defined by the velocity components u (x-direction) and v (y-direction), see Eq. (5). To determine the averaged flow angle ε_{avg}, the flow angle ε_{loc} is averaged over the width b at the narrow section, as shown in Eq. (6). For the investigation, the flow angle is calculated at $y = y_0 = 0$, the position of the narrow section.

$$\varepsilon_{loc} = \operatorname{atan}\left(\frac{v}{u}\right) \tag{5}$$

$$\varepsilon_{avg} = \frac{1}{b}\int_{-b/2}^{b/2} \varepsilon_{loc}(y_0, x)\,dx \tag{6}$$

In **Figure 4**, the flow angle ε_{loc} in the narrow section over the opening coordinate x is shown. The left diagram clarifies the profile of the flow angle between the left and right edges of the narrow section. Due to the Neumann (no slip) boundary conditions along a wall, the flow angle at the edges is equal or very similar to the orientation of the wall. On the left wall the geometrical angle α_l is 25 ° and the the flow angle is about 45 °. On the right side the geometrical angle α_r is 60 ° and the flow angle is about 108 ° (related to α_r 72 °). The deviations are caused by a strong rotation of the flow in the corners of the narrow section. The averaged value of the angle is ε_{avg} =79 °.

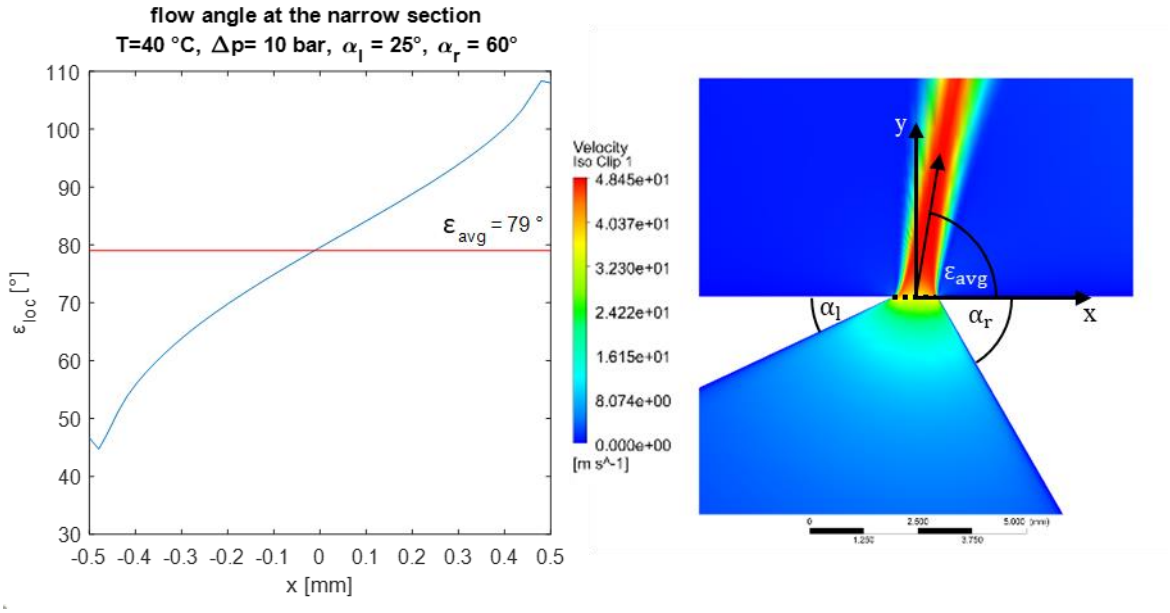

Figure 4: Flow angle ε_{loc} at the narrow section for the case: $\alpha_l = 25$ °, $\alpha_r = 60$ °, $\Delta p = 10$ bar, flow angle plotted over the opening coordinate x (left), velocity field of the free jet around the narrow section (right)

3.2. Laminar and turbulent influence

In this section the range of validity of the calculation of the averaged flow angle ε_{avg} for different Reynolds numbers is investigated. Decisive here is the consideration of a laminar and / or turbulent flow. According to [12] with reference to [13], the critical Reynolds number of a free jet is $Re \approx 30$. The Reynolds number is defined here as follows.

$$Re = \frac{\tilde{u} \cdot l}{\nu} \text{ with } \nu = \frac{\eta}{\rho} \tag{7}$$

The velocity $\tilde{u}$ is defined such as the characteristic length $l = b$ at the narrow section of the free jet. The Eq. (7) is illustrated by following example. A valve of nominal size 08 according to ISO 7368 is opened to 20 % and operates with a volume flow of 15 l / min. According to [14], this area of the valve is strongly in the laminar region of hydraulic resistance. The calculated Reynolds number Re = 138 is well above the critical value of 30. That means the flow is nevertheless predominantly laminar in the gap per se. Due to the superposition of laminar and turbulent flow, the resulting free jet behind the narrow section is nevertheless turbulent. It is clear there is a strictly separation between the laminar and turbulent behaviour of a hydraulic resistance and the characteristics of a free jet.

In the following, it will be shown that a turbulent free jet is almost always present for hydraulic components. This also applies to the minimal model. With the fluid properties of HLP 46 (**Table 1**), the following course of the Reynolds number over the pressure drop is obtained for the geometry, see **Figure 5**. In the diagram on the left, the Reynolds number is plotted against the pressure drop Δp. It includes the marked operating points investigated for this study. In order to gain a better understanding of the influence of temperature on the Reynolds number and thus on turbulence, the characteristic curve for 20 °C and 100 °C is shown in addition to the 40 °C curve. It shows that an undercutting of the limiting $\mathrm{Re} \approx 30$ (red line) is given even at lower temperatures like 20 °C for pressure drops smaller than 1 bar. A classical hydraulic application has much higher operating points. It shows that a laminar flow is only important in special cases of very low pressure drops and over large narrow sections. However, in such special cases effects like flow forces are negligible compared to static pressure forces. The reason for these cases with very low velocities is the quadratic contribution of the flow force, see Eq. (3).

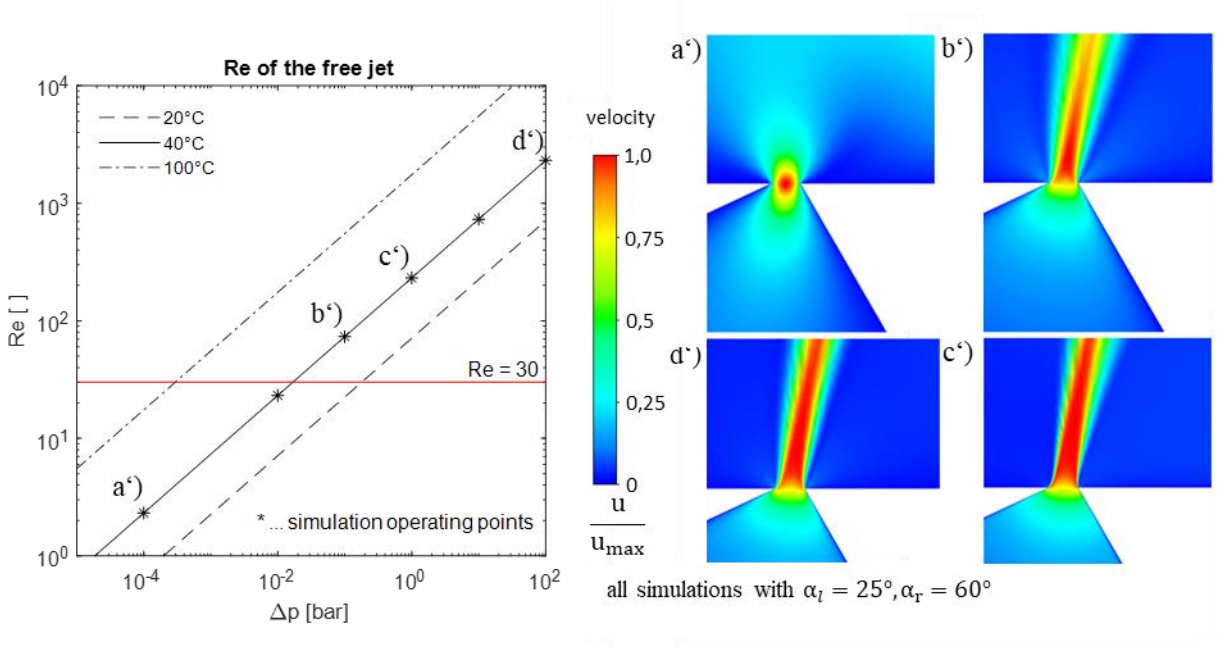

Figure 5: Investigation of the laminar-turbulent influence for the case: ”$\alpha_l = 25°$, $\alpha_r = 60°$„ Reynolds number plotted over pressure drop for various temperatures (left), velocity fields of the free jet for Reynolds numbers at a’) to d’)

On the right side in **Figure 5**, the velocity fields for the operating points a’) to d’) are shown for the geometrical inlet shape configuration from **Figure 4** ($\alpha_l = 25\,°$, $\alpha_r = 60\,°$). It can be seen how the shape of the free jet is influenced by increasing Reynolds number. For $\mathrm{Re} > 30$ the shape of the free jet is fully developed and has a sharp separation between the free jet velocity field and the static environment. For $\mathrm{Re} < 30$ the shear layer has almost disappeared and it prevails a laminar flow.

The correlation between the averaged flow angle ε_{avg} against the Reynolds number for various geometrical inlet shape configurations (α_l, α_r) will be discussed in **Figure 6**. The left diagram illustrates the normalized averaged flow angle $\varepsilon_{avg}/\varepsilon_{avg100bar}$ (normalized to turbulent flow) against the Reynolds number. A deviation is recognizable between the turbulent and the laminar flow for all cases. With exception of the case „$\alpha_l = 30\,°$, $\alpha_r = 140\,°$” for $\mathrm{Re} > 30$ all averaged flow angles stay almost the same and converge. Only for $\mathrm{Re} < 30$ it deviates up to 10 % of the

reference value. The reason for that is the influence of the laminar flow. The special case "$\alpha_l = 30\,°, \alpha_r = 140\,°$" already shows a much higher deviation at larger Reynolds numbers. For better understanding, the right side of the figure shows the configuration for cases a") to d") by increasing Reynolds numbers. Due the very flat inlet the free jet is attached to the wall even if the flows is turbulent. This effect is called Coanda effect, [12] and [15]. For certain inclinations of the free jet to the wall the suction area of the free jet leads to the fact that the free jet is aligned with the wall, [14] and [15]. For inlet shape configurations in this range, larger deviations are to be expected.

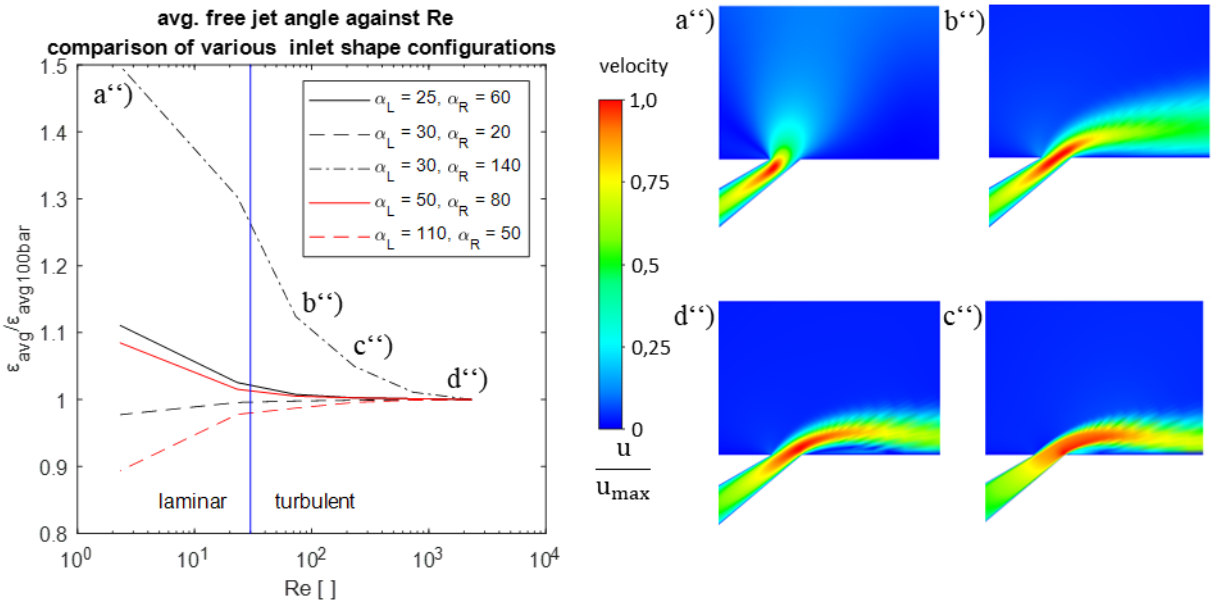

Figure 6: Averaged flow angle ε_{avg} against the Reynolds number for various geometrical inlet shape configurations (α_l, α_r, left), the influence on acute and flat boundary cases (right)

In summery, most important for hydraulic applications is the turbulent free jet. In contrast to the hydraulic resistance description the laminar and turbulent behavior of a flow is always considered in parallel as principle of superposition, as shown in [1]. The current investigation focuses on the free jet angle. The flow resistance of hydraulic components is not taken into account. Thus, it must not be confused with the laminar free jet at this point.

Because of its predominantly turbulent behavior, all further considerations are performed for the turbulent free jet.

3.3. Analytical method for the averaged flow angle

The derivation of the averaged flow angle ε_{avg} for a turbulent free jet is illustrated in **Figure 7**. In a) it can be seen an overview of the geometry near the narrow section including the inlet and outlet momentum. The momentum in the inlet is aligned according to the flow angle. The range of the flow angle is limited through geometrical parameters α_l and α_r. The right side (b) shows the course of the flow angle along the narrow section (see **Figure 4**). Regarding to ch. 3.1 the averaged flow angle lies in the center point of the narrow section. Additionally the course of $\varepsilon(x)$ can be separated in two parts. The first one $\varepsilon(x)^*$ is a point symmetrical graph with its center

point in the coordinate origin. The second part is a constant offset ε_{avg}. In summary the equation for $\varepsilon(x)$ is:

$$\varepsilon(x) = \varepsilon(x)^* + \varepsilon_{avg} \tag{8}$$

It is necessary to set an unproven but plausible assumption to make a reference to the momentum. The absolute value of the momentum over the flow angle in the inlet is uniform. Thus, the momentum can be written as $\vec{I}(\varepsilon) = \vec{e}(\varepsilon)|\vec{I}|$. In this formula $\vec{e}(\varepsilon)$ is the unit vector with the direction of ε. That means the whole fluid in the inlet moves uniformly towards to the narrow section.

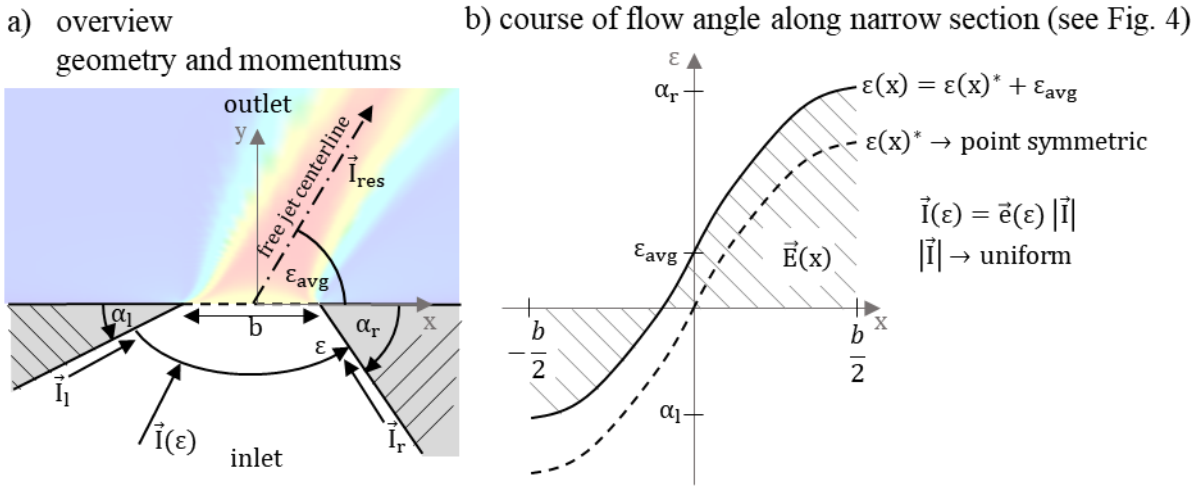

Figure 7: Prediction of the averaged flow angle ε_{avg} – simplified model to consider the incoming and outgoing momentum (a), course of the flow angle along the narrow section (b)

In the following, the relationship between the averaged flow angle and the geometry is derived from the assumptions just mentioned. Regarding to Eq. (6) the first mean value theorem is applied to the whole course of ε according to **Figure 7** b). Integrating over the graph of $\varepsilon(x)$ yields the following expression.

$$\varepsilon_{avg} = \frac{1}{b}\int_{-b/2}^{b/2} \varepsilon(x)\,dx = \frac{1}{b}[E(b/2) - E(-b/2)] \tag{9}$$

In this case E is the root function of ε. With the possibility to separate $\varepsilon(x)$ such as in Eq. (8), Eq. (9) can be extended and rearranged.

$$\varepsilon_{avg} = \frac{1}{2}\left[\left(\frac{E(b/2)^*}{b/2} + \varepsilon_{avg}\right) - \left(\frac{E(-b/2)^*}{b/2} - \varepsilon_{avg}\right)\right] \tag{10}$$

The expression $(.)^*$ symbolizes the point symmetrical part of the course. The separation remains in the root functions. The first term $\frac{E(\pm b/2)^*}{b/2}$ describes the mean increase of the function for the respective interval $[0,\, b/2]$ (case 1, left term) and $[-b/2,\, 0]$ (case 2, right term). The second part is only the offset. Both formula have the same structure like Eq. (8). By means of case separation between the two intervals case 1 and case 2, Eq. (8) can be integrated into Eq. (10).

In case 1 with the interval $[0, b/2]$, a linear equation is set up, which is to be determined at x = b/2. The increase of the function is defined over the whole interval with $\Delta E/\Delta x$. The offset is clarified through ε_{avg}. Case 2 can be described analogously. Eq. (11) shows for both intervals the expression in the form of Eq. (8).

$$\begin{aligned} \tilde{\varepsilon}(b/2) &= \frac{E(b/2)^* - E(0)}{b/2} + \varepsilon_{avg} = k\varepsilon(b/2)^* + \varepsilon_{avg} \text{ for } [0, b/2] \\ -\tilde{\varepsilon}(-b/2) &= \frac{E(0) - E(-b/2)^*}{b/2} - \varepsilon_{avg} = -k\varepsilon(-b/2)^* - \varepsilon_{avg} \text{ for } [-b/2, 0] \end{aligned} \tag{11}$$

The additional factor k is a scaling of the point symmetrical part of $\tilde{\varepsilon}$ for integrating of Eq. (8). With Eq. (11) it is possible to extend Eq. (10) to the following expression.

$$\varepsilon_{avg} = \frac{1}{2}[\tilde{\varepsilon}(b/2) + \tilde{\varepsilon}(-b/2)] \tag{12}$$

Because of the point symmetrical characteristic of $\tilde{\varepsilon}(x)$ as well as $\varepsilon(x)$ the term $\varepsilon(x)^*$ will always eliminate itself. The offset ε_{avg} remains and the Eq. (12) is fulfilled. Thus, Eq. (12) is universal for all point symmetrical equations with a uniform offset.

That means for calculations of the flow angle at the narrow section, only the flow angle at the limiting walls must be known. Regarding to **Figure 4** and the Neumann boundary conditions along a wall the flow angle and the local geometrical angle can be equated. It applies: $\tilde{\varepsilon}(b/2) = \pi - \alpha_r$ and $\tilde{\varepsilon}(-b/2) = \alpha_l$. For a better illustration, Eq. (12) can be extended to a vector sum of the inlet momentum with the reference to the resulting momentum of the free jet. The assumption $\vec{I}(\varepsilon) = \vec{e}(\varepsilon)|\vec{I}|$ with $|\vec{I}|$ as uniform is applied over the inlet area. The **Figure 8** shows the relationship between the momentum of inlet and outlet.

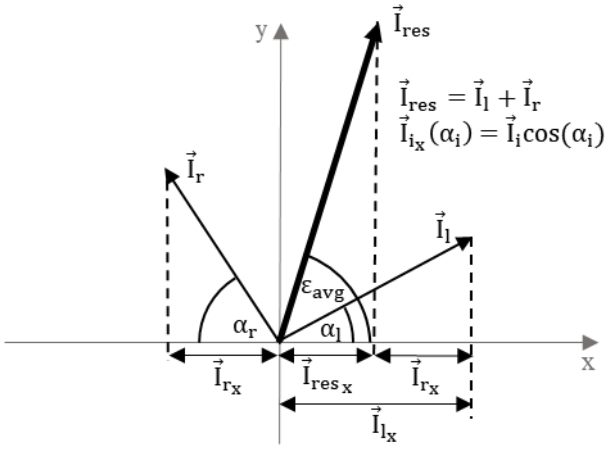

Figure 8: Momentum of inlet ($\vec{I}_l$ and $\vec{I}_r$) in reference to the outlet momentum $\vec{I}_{res}$

For the calculation, the relationship is transferred into Cartesian coordinates. With the expression $\vec{I}_{i_x}(\alpha_i) = \vec{I}_i \cos(\alpha_i)$ all angle dependent momentum can be related to the x component. The **Figure 8** illustrates sum of the x components aligned to the abscissa. According to this principle, Eq. (12) can be transferred into the x component of the Cartesian coordinates, as shown in Eq (13).

$$\cos(\varepsilon_{avg}) = \frac{1}{2}(\cos(\alpha_l) - \cos(\alpha_r)) \tag{13}$$

Equation (13) is the major finding of this work. It describes the correlation between the geometrical angles α_L, α_r and the averaged flow angle ε_{avg}. This equation allows the direct calculation of the flow angle from the geometry of the control edge only. It is independent of any operating conditions (see ch. 3.2). As an example, Eq. (13) gives a flow angle of 78,3 ° when the geometrical data from **Figure 4** are used. This matches very well with the CFD results of 79 °.

Figure 9 shows the comparison of the Eq. (13) and the CFD data over the full range of α_l and α_r. Geometrical impossible configurations, when $\alpha_l + \alpha_r > 180°$, are colored grey in the diagram. It can be seen that for all geometric shapes, the values calculated by Eq. (13) match very well with the CFD results. Only for the limiting cases $\alpha_l \gg \alpha_r$ as well as $\alpha_l \ll \alpha_r$ a slight deviation is observed. The deviations are smaller than 10 % for the special cases and thus acceptable. In another cases $\alpha_l = 0$ °and $\alpha_r = 0$ °, the free jet angle can only vary between 0 ° and 90 ° or from 90 ° to 180 °. If both inlet angles are identical, the free jet angle is always constant 90 °, as shown in the velocity field of configuration b'). This special case enables a symmetrical flow through the inlet geometry and generates a "classic" vertical free jet.

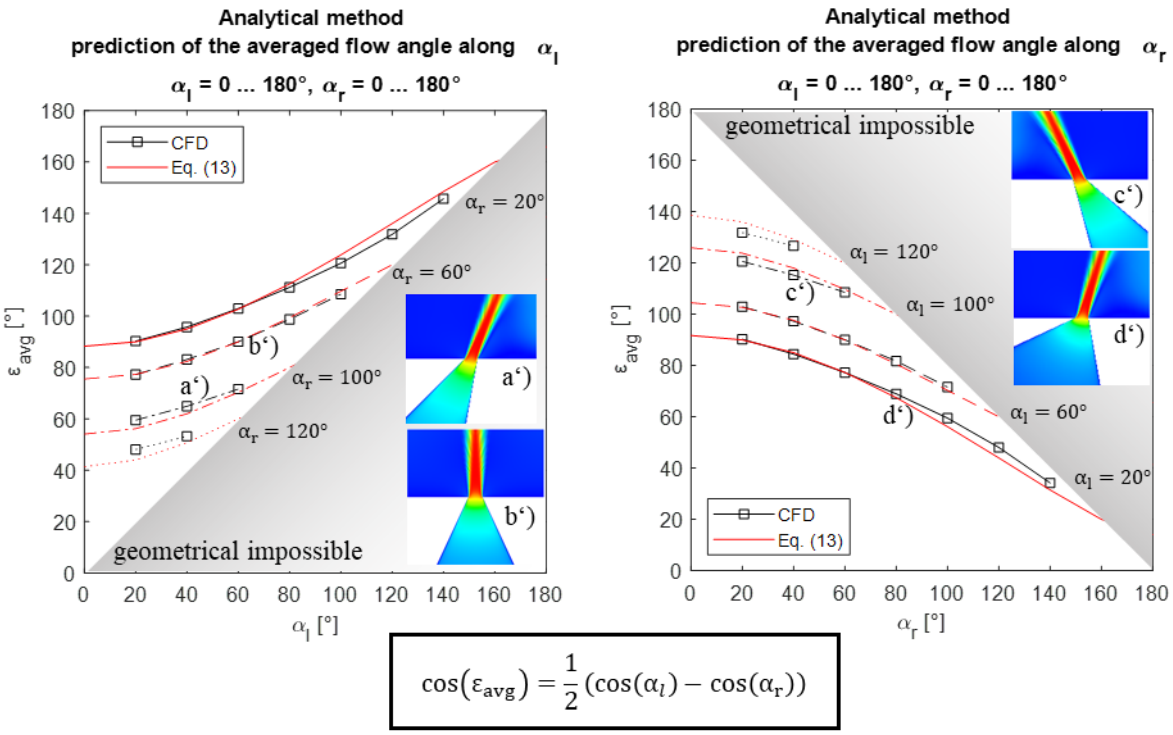

Figure 9: Prediction of the averaged flow angle ε_{avg} – comparison between Eq. (13) and CFD data, plotted over $\alpha_l = \{0 \ldots 180\}$ ° (left) and $\alpha_r = \{0 \ldots 180\}$ ° (right)

In summary, the Eq. (13) shows very good results compared to the minimal model. The simple expression represents a connection to geometrical parameters only and is not related to any operation conditions. The assumptions for this derivation is valid for turbulent flow. Thus, it is useable for almost all applications of hydraulic systems.

4. TRANSFER TO REAL APPLICATION

4.1. Prediction of the flow angle in real applications

In the following, the Eq. (13) is evaluated by using the rotary slide valve. **Figure 10** shows the comparison between CFD data with the results of Eq. (13). In a) the geometrical characteristics of the narrow section is defined. The influencing angle in the inlet of the valve is α_{in}. The angle α_{in} is valid in the range between 0 ° (vertical inlet) to 75 °. The relationship between α_{in} and the angles α_l and α_r of Eq. (13) is illustrated in figure a).

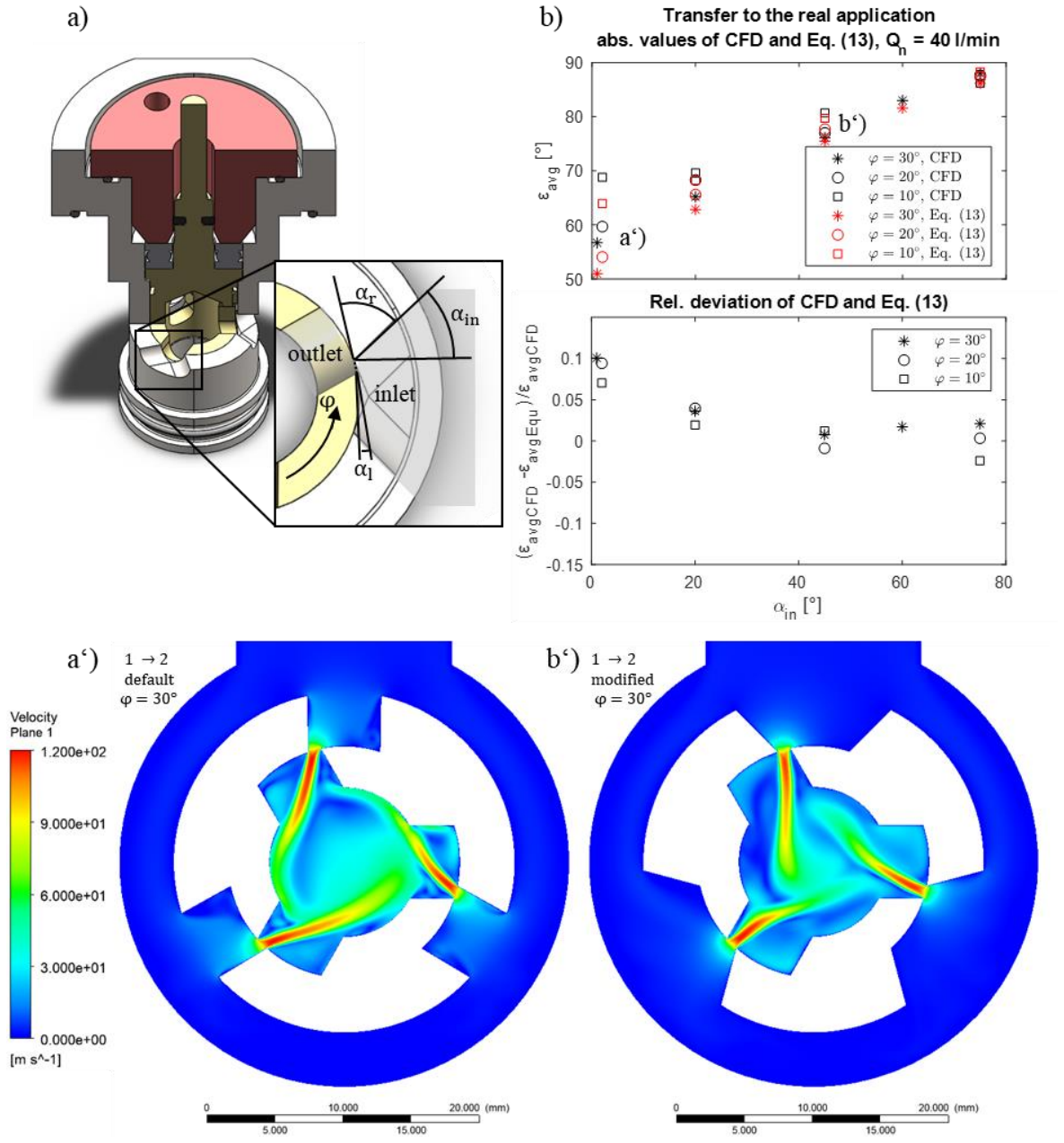

Figure 10: Rotary slide valve, geometrical setup (a), comparison between CFD data and the Eq. (13) along $\alpha_{in} = \{0 \dots 75\}$ ° for different twisting angles $\varphi = \{10,\ 20,\ 30\}$ ° (b), velocity field in symmetrical plane through the narrow sections for different configuration of $\alpha_{in} = \{0\ °,\ 45\ °\}$, $Q_n = 40$ l/min, flow direction $1 \rightarrow 2$ (see **Figure 1**)

The setup of all simulations is similar to **Table 1** and is expected to the parameter variation with α_{in}. In b) the absolute values of the averaged flow angle as well as the relative deviation between

CFD data and Eq. (13) are plotted over α_{in} for different twisting angles φ. The angle α_r corresponds to the inverse behavior of the angle α_{in} ($\alpha_r = 90\,° - \alpha_{in}$). Additionally, α_r and α_l have a variation from 0 ° (almost closed) to - 15 ° (almost fully open) dependent on the twisting angle. The reason for that is the convex shape of the outer surface of the valve spool. In order of the Eq. (13) to be applied, the geometric conditions must be established from **Figure 7**. Regarding to **Figure 9** right side, the graph of the absolute values shows a very similar course. For $\alpha_{in} > 20\,°$ the results between CFD and Eq. (13) match very well and the relative deviation is below 5 %. It proves that the explained calculation method is reliable. In the range of $\alpha_{in} < 20\,°$ the scattering of the values becomes larger between different twisting angles and the relative deviation is the highest in this course with about + 10 %. However, for an engineering application the deviations are still acceptable. The results in general are in line with the statement from **Figure 9**.

For a better understanding how the fluid domain is modified, in a') and b') the velocity field in a symmetrical plane through the narrow sections is shown for different configurations of $\alpha_{in} = \{0\,°,\ 45\,°\}$. The plot a') shows the default configuration with a vertical inlet. The free jets flow much more flatly into the geometry and have large contact regions with the wall. The second one, b'), clarifies the modified inlet shape. The free jets meet in the center and partially dissipate themselves. Thus, the resistance torque can be significantly reduced (see ch. 4.2). It is recognizable how α_{in} influence the flow angle of the free jet.

To sum up, the new method of Eq. (13) allows a reliable prediction of the flow angle of free jets. Same results can be achieved for complex geometries as the rotary slide valve. It is possible to influence actively the jet direction after the narrow section. Looking at other issues such as cavitation collapse regions (erosion regions) or stagnation points in general, the potential for improvement using Eq. (13) is high.

4.2. Improvement of the rotary slide valve

The main goal of the improvement of the valve is the reduction of the resistance torque which is strongly dependent on the flow force. As shown in Eq. (3) the flow force is mainly influenced by the flow angle at the narrow section. With the results of ch. 4.1, the following improvements could be made, as shown in **Figure 11**. The characteristic curves for pressure drop (a) and the resistance torque (b) over φ are plotted for the default (black) and the modified (red) valve design and both flow directions (see **Figure 1**). The direction $1 \rightarrow 2$ is marked as solid line and $2 \rightarrow 1$ as dashed line. In addition, both characteristic curves are simulated by a constant nominal flow rate Q_n. Comparing to pressure drop across φ (a), the results for both designs are similar. Moreover, the gradient is almost identical. There is only an angular offset of 1 ° to 2 °. Significant changes can be seen in the resistance torque. Especially for the flow of $1 \rightarrow 2$, the amount in the maximum range decreases by 65 % from 0.23 Nm to 0.08 Nm. The resistance torque of $2 \rightarrow 1$, on the other hand, is negatively affected. However, this effect is significantly smaller and can be accepted at this point. In order to actively influence the flow direction $2 \rightarrow 1$, the inlet angle of the inner geometry of the rotary slide valve would have to be varied according to this principle. Unfortunately, cost-related changes are not acceptable for cost optimized part usage in industrial applications.

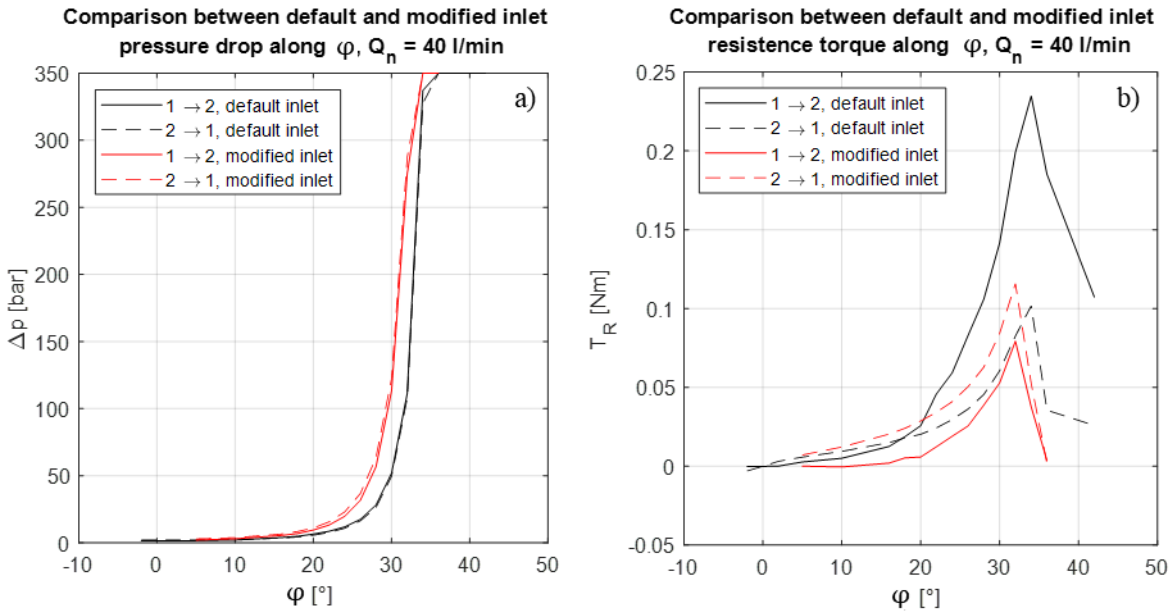

Figure 11: Improvement of the modification, comparison of the pressure drop across φ at constant flow rate (a) and of the resistance torque across φ (c), in each case for both flow directions, $Q_n = 40\ l/min$

In summary, the flow force improvement by using flow angle modification according to Eq. (13) is very effective. The main setup of the geometry is unchanged and only the inlet shape near the narrow section has to be modified. The impacts of this modification are enormous and the production effort is kept within limits.

5. DISCUSSION AND CONCLUSION

In summary, the following conclusions could be drawn with the help of the presented research.

Turbulent-laminar operating conditions

For turbulent flows, the averaged flow angle is independent of the operating point. In the range of laminar flows there is a clearly deviation compared to turbulent flow angles. Due to the low Reynolds number of Re ≈ 30, this effect is outside the operating conditions of "classical" hydraulic applications. Therefore, the operating range is always in the turbulent range and a behavior independent of the operating point is to be expected.

Analytical method for the determination of the flow angle

The new method according to Eq. (13), the averaged flow angle can be predicted with very good approximation. Slight deviations are only to be expected in ranges of $\alpha_l \gg \alpha_r$ as well as $\alpha_l \ll \alpha_r$, which can amount to a maximum deviation of 10 %. The simple expression represents only a dependency to geometrical parameters and is not related to any operation conditions. The assumptions for this derivation is valid for turbulent flow. Thus, it is useable for almost all applications of hydraulic systems.

Transferability to real applications

The new method of Eq. (13) allows a reliable prediction of the flow angle of free jets which is also applicable for a wide range of hydraulic geometries. It is possible to influence actively the

jet direction after the narrow section. Looking at other issues such as cavitation collapse regions (erosion regions) or stagnation points in general, the potential for improvement using Eq. (13) is high. The main setup of the geometry is unchanged and only the inlet shape near the narrow section has to be modified. The impacts of this modification are enormous and the production effort is kept within limits.

NOMENCLATURE

A	Area	m^2
b	width	m
f	acceleration	m / s^2
F	force	N
I	momentum	N s
l	characteristic length	m
n	normal vector	-
p	pressure	bar
r	radius	m
S	boundary of control volume	m^2
t	time	s
T	temperature	°C
T_R	resistance torque	Nm
u	velocity as vector or as component in x-direction	m / s
v	velocity as component in y-direction	m / s
V	volume	m^3
x	coordinate direction	m
y	coordinate direction	m
α	geometrical angle	°
Δ	difference	-
ε	flow angle	°
E	Root function of ε	
η	dynamic viscosity	Pa s
$\boldsymbol{\rho}$	density	kg / m^3
$\boldsymbol{\tau}$	shear stress tensor	Pa
υ	kinematic viscosity	mm^2 / s
φ	twisting angle	°
$\boldsymbol{\Omega}$	control volume	m^3

ACKNOWLEDGMENTS

The author would like to thank the institutions Bundesministerium für Bildung und Forschung (BMBF) and Europäische Union - NextGenertionEU for funding the project " Erarbeitung funktionsintegrierter Schaltventile für Maschinen, Anlagen und Fahrzeuge zur Senkung des Energieverbrauchs (funkiS)“with the funding code 01LY2004B.

REFERENCES

[1] N. Gebhardt, J. Weber (2020) Hydraulik – Fluid-Mechatronik. Grundlagen, Komponenten, Systeme, Messtechnik und virtuelles Engineering. Dresden, January 2020, Dresden, Germany

[2] S. Osterland, L. Günther, J. Weber (2022) Experiments and Computational Fluid Dynamics on Vapor and Gas Cavitation for Oil Hydraulics, TU Dresden, 2022 Dresden, Germany
[3] S. Osterland, L. Müller, J. Weber (2021) Influence of Air Dissolved on Hydraulic Oil on Cavitation Erosion, TU Dresden, 2021 Dresden, Germany
[4] R. Ivantysyn, A. El Shorbagy, J. Weber (2018) Schlussbericht – Smart Pump – decentralized control for vessel engine. Dresden, 2018, Dresden, Germany
[5] M. Dietze, et. al. (1996) Messungen und Berechnungen der Innenströmung in hydraulischen Sitzventilen. Technische Hochschule Darmstadt, 1996, Darmstadt, Germany
[6] M. Kipping, et. al. (1997) Experimentelle Untersuchungen und numerische Berechnungen zur Innen strömung in Schieberventilen in der Ölhydraulik. Technische Hochschule Darmstadt, 1997, Darmstadt, Germany
[7] C. Latour, et. al. (1996) Strömungskraftkompensation in hydraulischen Sitzventilen. RWTH Aachen, December 1996, Aachen, Germany
[8] M. Ristic, et. al. (2000) Dreidimensionale Strömungsberechnungen zur Optimierung von Hydraulikventilen bezüglich der stationären Strömungskräfte. RWTH Aachen, 2000, Aachen, Germany
[9] K. Wanne, et. al. (1965) Messung und Untersuchung der axialen Kräfte an ölhydraulische Steuerschiebern. Technische Hochschule Stuttgart, 1965, Stuttgart, Germany
[10] M. Lechtschewski, et. al. (1994) Untersuchung der Abhängigkeit der Strömungskraft vom Hub des Ventilschiebers und der Druckdifferenz. Institut für Werkzeugmaschinen und Fluidtechnik, TU Dresden, 1994, Dresden, Germany
[11] S. Osterland, J. Weber (2016) A numerical study of high pressure flow through a hydrsulic pressure relief valve considering pressure and temperature dependent viscosity, bulk modulus and density. TU Dresden, 2016 Florianópolis, Brazil
[12] H. Schlichting, K. Gersten (1996) Grenzschicht-Theorie. Springer-Verlag, 1996, Bochum, Germany, ISBN: 3-540-55744-x 9th edition
[13] E. N. Andrade, et. al. (1931) The velocity distribution in a liquid-into-liquid jet. The plane jet. Proc. Phys. Soc. London, 1931, London, UK
[14] J. Liu, A. Sitte, J. Weber, (2022) Invesitgation of temperature on flow mapping of electrohydraulic valves and corresponding applications, ASME/BATH 2022., UK
[15] E. Truckenbrodt (1980) Fluidmechanik – Band 2 Elementare Strömungsvorgänge, dichteveränderliche Fluide sowie Potential und Grenzschichtrömungen. Springer-Verlag Berlin Heidelber New York. München, Germany, ISBN 3-540-10135-7 2nd edition